ACS Energy LETTERS

http://pubs.acs.org/journal/aelccp

Breeze-Wind-Energy-Powered Autonomous Wireless Anemometer Based on Rolling Contact-Electrification

Xianpeng Fu,[#] Shaohang Xu,[#] Yuyu Gao, Xiaohan Zhang, Guoxu Liu, Han Zhou, Yi Lv, Chi Zhang,* and Zhong Lin Wang*

Cite This: ACS Energy Lett. 2021, 6, 2343–2350

Read Online

ACCESS | Metrics & More | Article Recommendations | Supporting Information

ABSTRACT: A triboelectric nanogenerator (TENG) has great advantages in harvesting low-frequency mechanical energy, which is very suitable for energy harvesters and active sensors for breeze wind. Here, we report a breeze-wind-driven autonomous wireless anemometer (W-WA) based on a planetary rolling triboelectric nanogenerator (PR-TENG) for simultaneous wind energy harvesting and wind speed sensing. Benefitting from the planetary rolling friction, the PR-TENG can be activated at a wind speed of less than 2 m/s. At a wind speed of 5 m/s, the W-WA can be continuously powered and autonomously transmit wind speed data in the range of 10 m every 2 min. By integrating the TENG-based micro/nanoenergy harvester and active sensor, this work has realized a complete self-powered intelligent wireless sensing system, which has exhibited broad prospects in distributed micro/nanoenergy, unattended environmental monitoring, and the Internet of things.

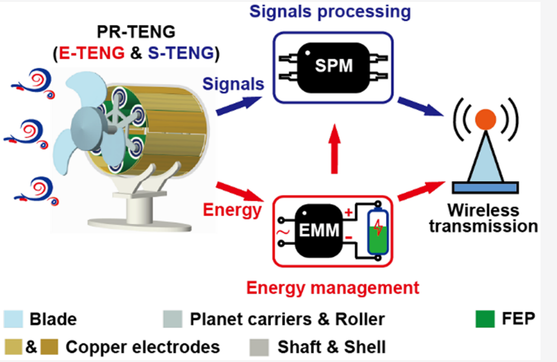

Wind as a kind of widely distributed and renewable energy has played a significant role in electric supply and contributed to alleviate the energy crisis.[1−6] According to statistics, the exploitable part of global wind energy is up to 5.3×10^{13} kWh per year.[7−9] On the other hand, the anemometer is a powerful device for wind monitoring and weather forecasting that usually works in unattended environment and needs a long service life. Up to now, the anemometer is mainly supplied by short-term battery, which greatly increases the maintenance cost and environmental pollution.[10−13] Therefore, harvesting wind energy from the ambient environment to power the anemometer is an optimal method to realize sustainable operation.

As a new energy technology, the triboelectric nanogenerator (TENG) based on Maxwell's displacement current was first proposed in 2012[14−16] and has been widely used as an energy harvester[17−20] and active sensor.[21−23] As an energy harvester, the TENG has a better output performance for harvesting low-frequency and weak mechanical energy compared to a traditional electromagnetic generator,[24−26] which can provide sustainable micro/nanopower sources for distributed electronic devices.[27−30] As an active sensor, the TENG-based active sensor has the advantages of being lightweight, high flexibility, and an abundant selection of materials compared with the electromagnetic- or piezoelectric-based active sensor.[7] Some TENG-based wind energy harvesters and sensors have been studied to harvest and monitor wind energy effectively.[31−34] Although the TENG-based active wind sensor can directly convert wind information into sensing electrical signal without a power supply,[35−37] the signal processing and transmission still need an external power supply for this kind of active sensor.[38] If a TENG-based wind sensor can be supplied by a TENG-based power source, it is very promising to realize a fully self-powered system for autonomous wind sensing.

Here, we report a breeze-wind-driven autonomous wireless anemometer (W-WA) based on a planetary rolling triboelectric nanogenerator (PR-TENG) for simultaneous wind energy harvesting and wind speed sensing. Benefitting from the planetary rolling friction, the PR-TENG can be activated at a wind speed of less than 2 m/s. The output electric energy from the PR-TENG can be managed as a power supply with a steady

Received: April 3, 2021
Accepted: June 1, 2021
Published: June 3, 2021

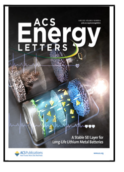

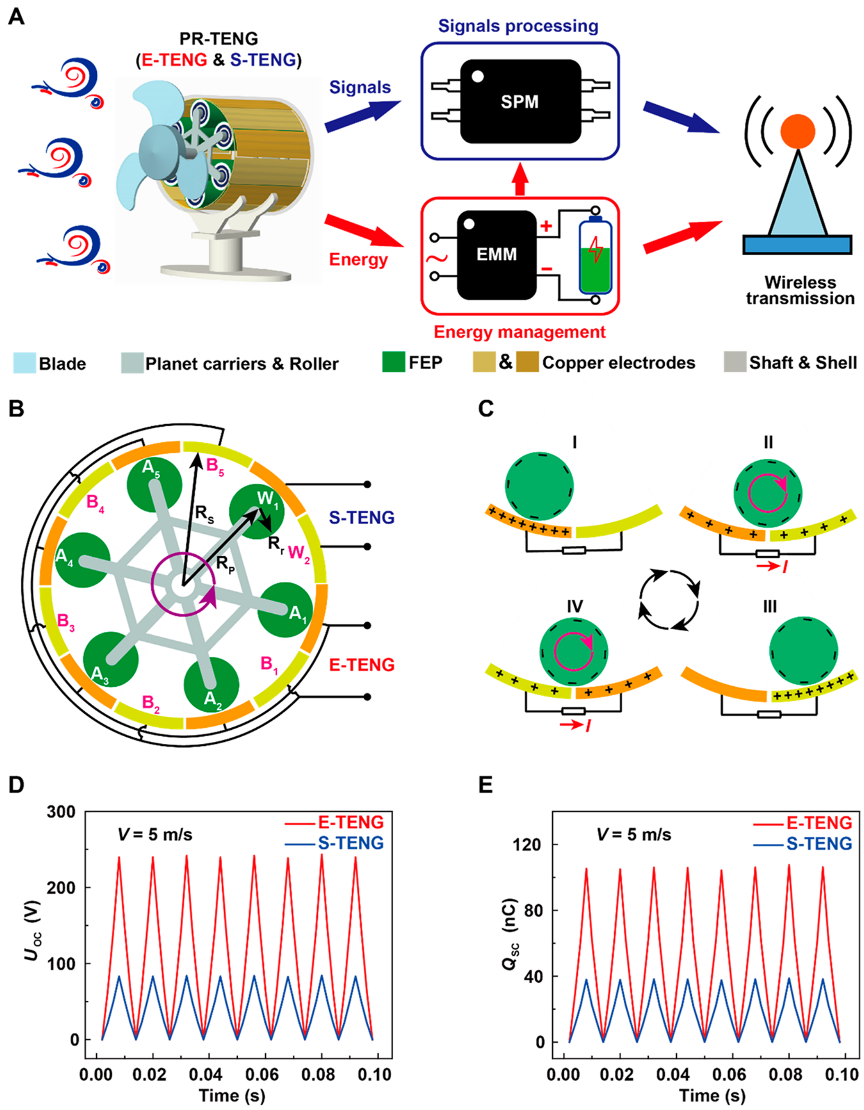

Figure 1. Basic structure and working mechanism of the wind-energy-powered autonomous wireless anemometer (W-WA). (A) Framework for the W-WA. The W-WA consists of a planetary rolling triboelectric nanogenerator (PR-TENG), signal processing module (SPM), and energy management module (EMM). (B) Schematic diagram showing the structural design of the stator and rotor. (C) Working principle of PR-TENG. (D) Open-circuit voltages of E-TENG and S-TENG at 5 m/s. (E) Short-circuit transfer charges of E-TENG and S-TENG at 5 m/s.

2.5 V voltage, while the output electric signals from the PR-TENG indicate the wind speed by frequency measurement and calculation. At a wind speed of 5 m/s, the W-WA can be continuously powered and autonomously transmit wind speed data in the range of 10 m every 2 min. By integrating the TENG-based micro/nanoenergy harvester and active sensor, this work has realized a complete self-powered intelligent wireless sensing system, which has exhibited broad prospects in distributed micro/nanoenergy, unattended environmental monitoring, and the Internet of things.

Figure 1 shows the basic structure and working framework of the autonomous W-WA powered by breeze wind energy. As shown in Figure 1A, the W-WA is composed of a PR-TENG, an energy management module (EMM), a signal processing module (SPM), and a transmitter. The PR-TENG with two output channels is employed to harvest wind energy and monitor wind speed simultaneously. The energy channel (E-TENG) and sensing channel (S-TENG) of the PR-TENG are connected with the EMM and SPM, respectively. For the wind energy harvesting, the E-TENG converts the wind energy into alternating-current (AC) electrical energy, and then, the AC electrical energy is managed by the EMM to provide a steady 2.5 V direct-current (DC) voltage for the SPM and transmitter. Meanwhile, for wind speed sensing, the S-TENG converts wind speed information into an electrical signal. Then, the electrical signal is regulated and analyzed by the SPM. Finally, the measured data are sent to the remote wireless receiving terminal through the transmitter. With the continuous breeze wind energy, the W-WA can sustainably and autonomously transmit measurement data.

As shown in Figure 1B, the PR-TENG is fabricated in a rolling free-standing mode with six pairs of finger copper electrodes. Five pairs (A_{1-5} and B_{1-5}) are connected in parallel and used as the output terminal of the E-TENG, and the other pair of electrodes (W_1 and W_2) serves as the output terminal of the S-TENG. The planet carrier and roller are fabricated by 3D printing. The fluorinated ethylene propylene (FEP) film is attached on the surfaces of the roller. When the W-WA is

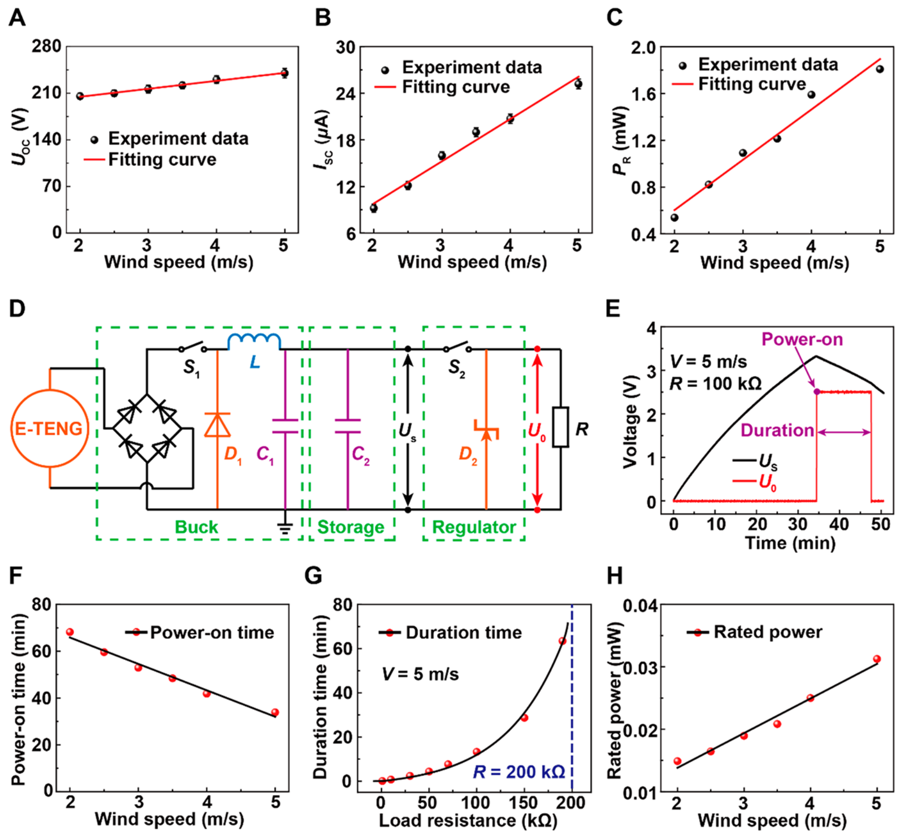

Figure 2. Electrical output and charging characteristics of the E-TENG. (A) Relationship between the output U_{OC} and wind speed. (B) Relationship between the output I_{SC} and wind speed. (C) Relationship between the output peak power and wind speed. (D) Circuit diagram of the EMM for the E-TENG. (E) The stored and steady voltage waveforms of the EMM with 100 kΩ load resistance at 5 m/s. (F) Charging time for a 15 mF capacitor to 3.3 V with different wind speeds. (G) The duration time of a 2.5 V regulated voltage with different load resistances at 5 m/s. (H) The rated output power of the EMM with different wind speeds.

driven by the breeze wind energy, the planet carrier can rotate counterclockwise, and the rollers roll clockwise on their own axis. Due to the rolling motion between the two triboelectric layers by using the planetary rolling structure, the friction force between the two triboelectric layers can be reduced. The dimension relationship of the stator shell, planet carrier, and roller can be expressed as $R_s = R_P + R_r$. The detail fabricated process is indicated in Materials and Methods. Benefitting from the almost negligible planetary rolling friction, the W-WA can be activated at a wind speed of less than 2 m/s. By coupling of contact-electrification and in-plane-rolling-induced charge transfer, the working principle of the PR-TENG is shown in Figure 1C. At the initial state, the rollers covered by FEP film contact with the electrode group A_{1-5} in the matching position, as shown in Figure 1C (I). Electrons will be transferred from copper surfaces to the FEP surfaces due to the different electronegativity.[39] Equal amounta of the positive and negative charges will be generated on the copper and FEP surfaces, respectively. In this state, there is no electron flow through the external circuit. When the rotor rotates counterclockwise driven by the wind, the rollers covered by FEP film will rotate clockwise on their own axis and gradually roll from the matching position with electrode group A_{1-5} to electrode group B_{1-5}, as shown in Figure 1C (II). The forward current flows from the electrode group A_{1-5} to the electrode group B_{1-5} driven by the potential difference for achieving a new electrostatic balance. Until the rollers reach the fully matching position with the electrode group B_{1-5}, nearly all of the positive charges on the electrode group A_{1-5} will be neutralized by the electrons from the electrode group B_{1-5}, as shown in Figure 1C (III). When the rotor continues to rotate counterclockwise to the electrode group A_{1-5}, the reverse current flows from the electrode group B_{1-5} to the electrode group A_{1-5} through the external circuit to reestablish the electrostatic equilibrium, as shown in Figure 1C (IV). Until the rollers arrive at the fully matching position with the electrode group A_{1-5}, all the electrons on the electrode group A_{1-5} flow back to the electrode group B_{1-5} and achieve the electrostatic equilibrium again, as indicated in state I. Electrons flow back and forth between the two electrode groups, generating an AC signal. When the W-WA is driven by the wind at 5 m/s, 239.75 and 83.11 V open-circuit voltages (U_{OC}) can be generated by the E-TENG and S-TENG, respectively, as shown in Figure 1D. And 105.31 and 38.37 nC short-circuit transferred charges (Q_{SC}) can be generated by the E-TENG and S-TENG, respectively, as shown in Figure 1E.

The electrical output characteristics of the E-TENG, as shown in Figure 2, are measured by an air bellow with a wind speed ranging from 2 to 5 m/s. Figure S1 shows the output open-circuit voltage waveforms of the E-TENG. As shown in Figure 2A, the peak-to-peak value of the U_{OC} increases from 205.45 to 239.98 V when the wind speed increases from 2 to 5 m/s. The output U_{OC} slightly increases with the increase of the wind speed. The possible reason is the contact force between the FEP layer and copper electrode increases with the increase of centrifugal force. Figure S2 indicates the output short-circuit

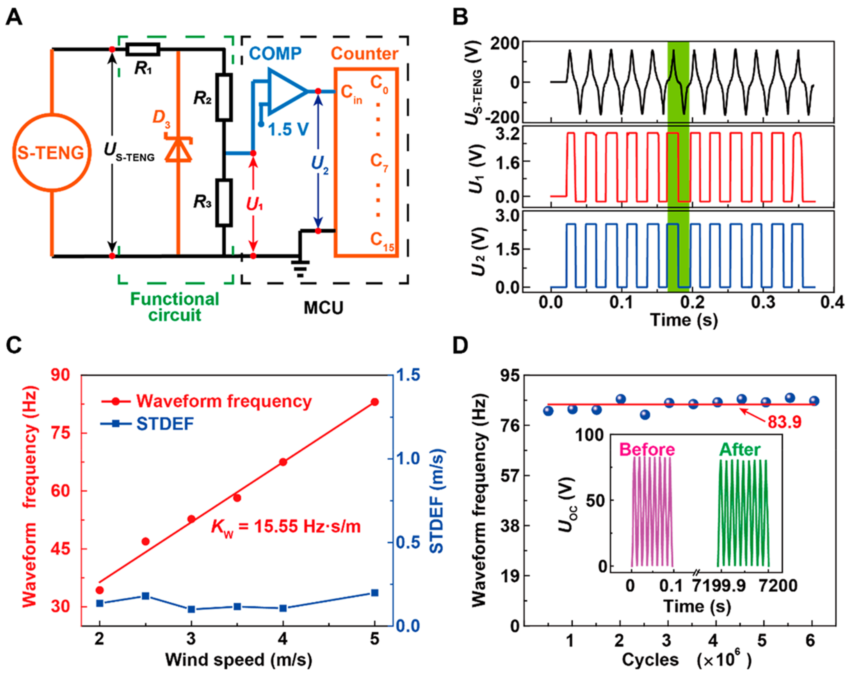

Figure 3. Wind speed monitoring mechanism and characteristics of the W-WA. (A) Schematic diagram of the wind speed sensing for the S-TENG. (B) Output signal comparation diagram between the S-TENG, signal regulator, and MCU. (C) The waveform frequency and standard deviation at different wind speeds. (D) Stability of the self-powered anemometer; the inset shows the U_{OC} of the S-TENG before and after 5 h at 5 m/s.

current (I_{SC}) waveforms of the E-TENG, which increases with the increase of the wind speed. The peak value of the I_{SC} increases from 9.19 to 25.18 μA when the wind speed increases from 2 to 5 m/s, as shown in Figure 2B. The impedance characteristics of the E-TENG at different wind speeds are systematically studied, as shown in Figure S3. At each wind speed, the instantaneous power initially rises and then drops, achieving a maximum value at 7 MΩ. As indicated in Figure 2C, the maximum values of the instantaneous power increase with the increase of wind speed. When the wind speed increases from 2 to 5 m/s, the maximum values of the instantaneous power increase from 0.54 to 1.81 mW. The E-TENG shows excellent durability, as shown in Figure S4. The open-circuit voltage is slightly decreased after 6×10^6 cycles at 5 m/s.

The output electrical energy of the E-TENG is regulated with the EMM to provide a steady 2.5 V DC voltage for the SPM and transmitter. Figure 2D indicates the circuit diagram of the EMM, which consists of a buck circuit, storage capacitor, and regulator. The buck circuit consists of a full-bridge rectifier, serial switch S_1, inductor L, parallel freewheeling diode D_1, and capacitor C_1, which are employed to adjust the voltage and impedance of the E-TENG. When S_1 is turned on under the control by the voltage of the E-TENG, the output electricity of the E-TENG is temporarily stored in the L-C_1 unit with the snap-off D_1. When the S_1 is turned off, the temporary stored energy in the L-C_1 unit is transferred to the storage capacitor C_2 with the opened D_1. With the continuous operation of S_1, the output electrical energy of the E-TENG can be maximally stored in C_2. The EMM is designed with L = 2.4 mH, C_1 = 10 μF, and C_2 = 15 mF. The charging efficiency can be more dramatically improved with the EMM than with the rectifier. As shown in Figure S5, the stored voltage U_S can achieve 1.28 V with the EMM after 10 min of charging, while the U_S is only 0.33 V by direct charging. The stored voltage U_S can be controlled by the regulator, which consists of a switch S_2 and a voltage stabilizer D_2. When U_S achieves a certain value, S_2 is turned on, and U_0 is pulled up from zero to a steady voltage. Based on the EMM, the pulse voltage of the E-TENG can be transferred into a steady DC voltage and power for the SPM and transmitter.

Figure 2E shows the waveforms of the U_S and U_0 with a 100 kΩ load resistance at 5 m/s. When the U_S exceeds 3.3 V, the switch S_2 is powered on immediately, and the U_0 is pulled from 0 to 2.5 V. At the continuous output electricity of the E-TENG, the U_0 will be pulled down from 2.5 to 0 V after a certain duration time due to the energy consumption on the load resistances. The power-on time with the different wind speeds are indicated in Figure S6 and summarized in Figure 2F. The power-on time reduces with the higher wind speed. When the load resistances are different, the duration times of the U_0 = 2.5 V are different. As shown in Figure 2G, the longer duration time can be maintained with the larger load resistances at 5 m/s. When the load resistances $R \geq 200$ KΩ, U_0 can be kept at 2.5 V all the time. Therefore, the rate output power of the EMM can be calculated according to the equation $P_e = \frac{U_0^2}{R}$. The rate output power with different wind speeds is summarized in Figure 2H, which indicates the EMM can provide a larger rate output power with faster wind.

Figure 3 shows the wind speed monitoring mechanism and characteristics of the W-WA. The S-TENG is connected with the SPM to monitor the wind speed. When the W-WA is driven by the wind, the SPM can measure the wind speed by counting the signal frequency of the output voltage from the S-TENG. Compared with the peak value of the output voltage, the waveform frequency can better indicate wind speed. The peak value of the output voltage is fluctuating due to the unsteadiness of the surface triboelectric charge quantity, while the waveform frequency measurement can avoid the influence

https://doi.org/10.1021/acsenergylett.1c00704
ACS Energy Lett. 2021, 6, 2343−2350

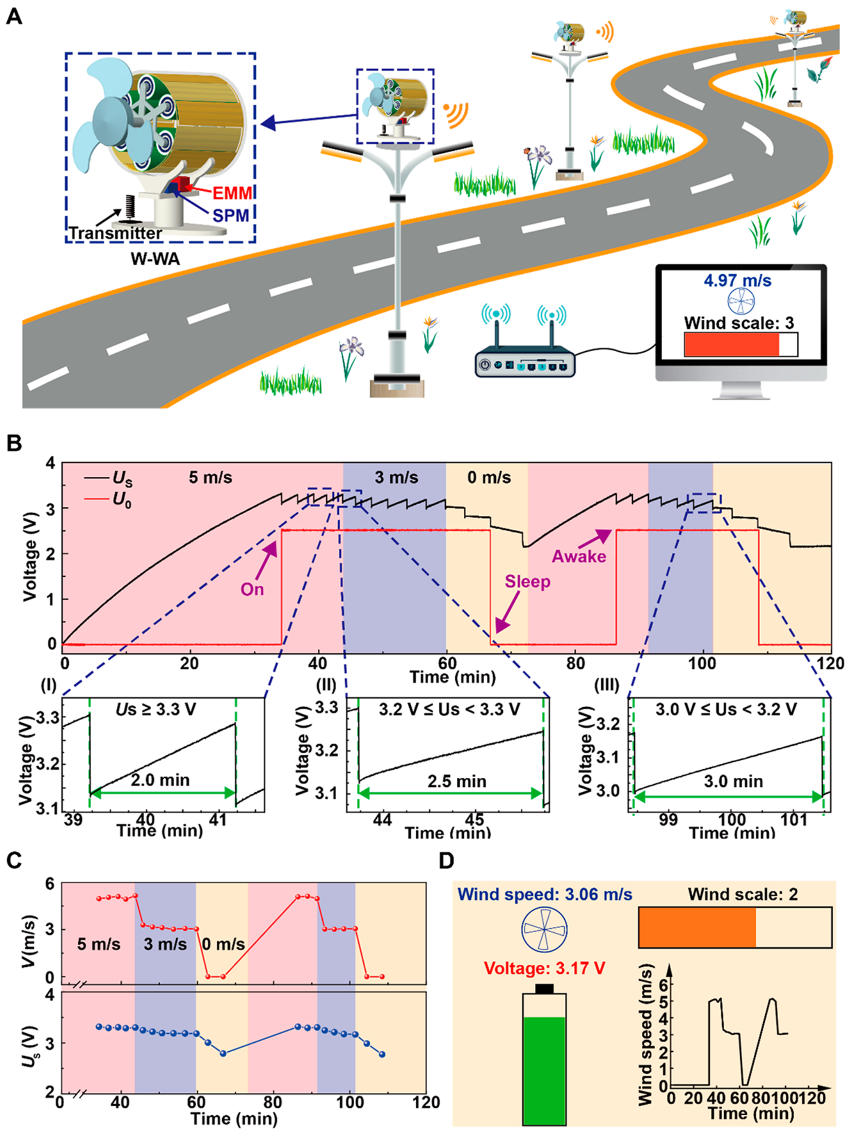

Figure 4. Application for autonomous and sustainable wireless sensing and data transmission driven by wind energy. (A) Sketch of the W-WA for wind speed monitoring. (B) The voltage variation of the capacitor connected with the EMM for several consequent transmitting cycles. (C) The received data of wind speed and voltage. (D) The display interface of the wireless receiving terminal.

of this fluctuation. Figure 3A indicates the circuit diagram of the SPM. The SPM consists of a functional circuit and microprogrammed control unit (MCU). The functional circuit is composed of a resistor R_1, a parallel Zener diode D_3, and two serial resistors R_2 and R_3, which are used to convert the pulse voltage signals of S-TENG into a detectable DC voltage signal. The MCU is employed to analyze the wind speed information from the functional circuit. The reference voltage of the comparator is set to 1.5 V, which is divided from the 2.5 V DC voltage supplied by the E-TENG. When the W-WA is driven by the wind, the pulse voltage signals of S-TENG are converted into a DC voltage signal maintaining a same frequency by the Zener diode. Once the voltage U_1 across the resistor R_3 exceeds the 1.5 V reference voltage, the comparator outputs voltage U_2 and the count increases by one in the counter. With the continuous working of the S-TENG, the wind speed information can be obtained by the MCU according to the count in the counter. The voltage waveforms of the $U_{\text{S-TENG}}$, U_1, and U_2 are summarized in Figure 3B, and their frequencies maintain a good consistency. In the output voltage waveform, each pulse signal of $U_{\text{S-TENG}}$ (highlight in green) is converted into a 5.2 V square wave by the Zener diode D_3, and the 2.88 V square wave U_1 is obtained by dividing it from the 5.2 V square wave. Figure 3C indicates the waveform frequency and standard deviation curve with different wind speeds. The signal frequency has a great linear relationship with the wind speed, indicating that it has superiority for wind speed sensing. The sensitivity of the W-WA can achieve 15.55 Hz·s/m. The W-WA has excellent measurement accuracy, in which the maximal standard deviation is 0.19 m/s with 30 repeated measurements at each different wind speed. The durability of the W-WA is also investigated, as shown in Figure 3D. The waveform frequency of the U_{OC} can steady at 83.9 Hz during the 6×10^6 cycles at 5 m/s. The W-WA exhibits excellent durability.

With the simultaneous wind energy harvesting and sensing, the W-WA can realize the autonomous and sustainable wireless wind speed sensing and data transmission, as shown in Figure 4. The EMM, SPM, and transmitter are integrated with the PR-TENG and indicates a potential application of W-WA for wind speed monitoring with an unattended and long life, as shown in Figure 4A. Figure S7 shows a simulated wind environmental experiment for the W-WA. The W-WA is driven by an air bellow, and a laptop connected with a receiver is employed as the display terminal 10 m away. The photos of the EMM and SPM are shown in Figure S8. The voltage waveforms of U_S and U_0 are indicated in Figure 4B when the W-WA is driven by the wind with different speeds. In the starting state, both the U_S and U_0 are 0 V. When the W-WA is started by the wind at 5 m/s, the value of the U_S is increasing to 3.3 V in 34.2 min. At the same time, U_0 is stabilized to 2.5 V, and the U_S immediately drops to 3.12 V, indicating 8.67 mJ of energy is consumed for activating the SPM. The W-WA power-on process is indicated in Movie S1. After activation, the U_0 can be maintained at 2.5 V regardless of the voltage variation of U_S. The sampling and transmitting period of the wind speed data are controlled by the MCU according to the U_S, which is also periodically monitored by the MCU, and the U_S data is sent for showing the surplus energy. The data are transmitted with 8 bytes and 8.44 mJ of energy consumption. When the W-WA is excited in 5 m/s, U_S can remain above 3.3 V for the balance between the wind energy harvesting and power consumption in the W-WA. The wind speed and U_S data are sampled and transmitted every 2 min, as shown in Figure 4B(I) and Movie S2. While when the W-WA is excited at 3 m/s, U_S can remain above 3.2 V, and the cycle extends to 2.5 min, as shown in Figure 4B(II). The sampling and transmitting cycles are further extended to 3 min for saving energy when $3.0 \leq U_S < 3.2$ V, as shown in Figure 4B(III) and Movie S3. Once the wind speed decreases to 0 m/s, the energy stored in the capacitor C_2 is gradually consumed. Until the U_S decreases to 2.7 V, the U_0 is back to 0 V, and the W-WA turns into the sleep state. If the W-WA is driven and U_S reaches 3.3 V again, the W-WA can be awake, and U_0 recovers to 2.5 V. As a demonstration, the receiving wind speed and U_S data during 120 min are summarized in Figure 4C. The display interface of the terminal is shown in Figure 4D, including the measurement wind speed and U_S data in real time as well as the calculated wind scale and historical wind speed data. The harvested energy by E-TENG can meet the energy consumption for processing, calculating, and transmitting the sensing signal from the S-TENG. With the continuous wind energy, the W-WA can sustainably and autonomously provide the monitoring data by wireless communication, which has broad prospects in distributed micro/nanoenergy, unattended environmental monitoring, and the Internet of things.

In summary, we have demonstrated a breeze-wind-driven autonomous W-WA based on a PR-TENG for simultaneous wind energy harvesting and wind speed sensing. Benefitting from the planetary rolling friction, the PR-TENG can be activated at a wind speed of less than 2 m/s. At different wind speeds, the output characteristics of E-TENG are investigated. The output maximum instantaneous power can achieve 1.81 mW at 5 m/s. The output electric energy from the E-TENG can be managed as a power supply with a steady 2.5 V DC voltage, which can provide a maximum rate power of 0.03 mW. The output electric signals from the S-TENG can indicate the wind speed by frequency measurement and calculation. The W-WA has excellent measurement accuracy, in which the maximal standard deviation is 0.19 m/s. By the autonomous monitoring mechanism, the data monitoring and transmitting cycles can be intelligently adjusted according to the stored energy. At a wind speed of 5 m/s, the stored voltage can be maintain above 3.3 V, and the W-WA can be continuously powered and autonomously transmit wind speed data in range of 10 m every 2 min. The harvested energy by E-TENG can meet the energy consumption for processing, calculating and transmitting the sensing signal from the S-TENG. By integrating the TENG-based micro/nano energy harvester and active sensor, this work has realized a complete self-powered intelligent wireless sensing system, which has broad prospects in distributed micro/nanoenergy, unattended environmental monitoring, and the Internet of things.

■ MATERIALS AND METHODS

Fabrication of the PR-TENG. The PR-TENG consists of an outer cylindrical shell, two planet carriers, and six rollers. The size of the outer shell is $\Phi 100 \times 100$ mm, while the radii of the planet carrier and roller are 37.2 and 12.75 mm. The planet carrier and roller are fabricated by 3D printing. Six pairs of copper electrodes that are 50 μm thick are fabricated with flexible circuit board printing technology, which is fixed at the inner wall of the cylindrical shell to form the stator. The FEP films that are 30 μm thick are attached on the surfaces of the roller. The six rollers are connected with two planet carriers by the bearing to form the rotor. The blade, shaft, and rotor are rigidly connected.

Characterization and Measurement. The air bellow is employed to provide a continuous and speed-controllable wind simulation environment for the W-WA. The software and hardware systems of the W-WA are based on Microsoft Visual Studio and a C8051f410 single-chip microcomputer, respectively. The display interface is designed based on Python software.

■ ASSOCIATED CONTENT

Supporting Information

The Supporting Information is available free of charge at https://pubs.acs.org/doi/10.1021/acsenergylett.1c00704.

Movie S1. The W-WA power-on and data transmission (AVI)

Movie S2. Data transmission in 2 min cycle at a higher stored energy level (AVI)

Movie S3. Data transmission in 3 min cycle at a lower stored energy level (AVI)

Figure S1. Output signals of U_{OC} of the E-TENG with different wind speeds; Figure S2. Output signals of I_{SC} of the E-TENG with different wind speeds; Figure S3. Calculated instantaneous power of the E-TENG with variable resistances; Figure S4. Durability test of the E-TENG at a wind speed of 5 m/s after 6×10^6 cycles; Figure S5. Comparison of direct and managed charging for the storage capacitor at 5 m/s of the E-TENG; Figure S6. The charging waveforms of the storage capacitor with different wind speeds of the E-TENG; Figure S7. Demonstration of the W-WA with an air bellow; Figure S8. The photos of the EMM and SPM (PDF)

■ AUTHOR INFORMATION

Corresponding Authors

Chi Zhang – *CAS Center for Excellence in Nanoscience, Beijing Key Laboratory of Micro-nano Energy and Sensor, Beijing Institute of Nanoenergy and Nanosystems, Chinese Academy of Sciences, Beijing 101400, China; School of*

https://doi.org/10.1021/acsenergylett.1c00704
ACS Energy Lett. 2021, 6, 2343−2350

Nanoscience and Technology, University of Chinese Academy of Sciences, Beijing 100049, China; Center on Nanoenergy Research, School of Physical Science and Technology, Guangxi University, Nanning 530004, China; orcid.org/0000-0002-7511-805X; Email: czhang@binn.cas.cn

Zhong Lin Wang – *CAS Center for Excellence in Nanoscience, Beijing Key Laboratory of Micro-nano Energy and Sensor, Beijing Institute of Nanoenergy and Nanosystems, Chinese Academy of Sciences, Beijing 101400, China; School of Nanoscience and Technology, University of Chinese Academy of Sciences, Beijing 100049, China; School of Material Science and Engineering, Georgia Institute of Technology, Atlanta, Georgia 30332, United States;* orcid.org/0000-0002-5530-0380; Email: zlwang@gatech.edu

Authors

Xianpeng Fu – *CAS Center for Excellence in Nanoscience, Beijing Key Laboratory of Micro-nano Energy and Sensor, Beijing Institute of Nanoenergy and Nanosystems, Chinese Academy of Sciences, Beijing 101400, China; School of Nanoscience and Technology, University of Chinese Academy of Sciences, Beijing 100049, China*

Shaohang Xu – *CAS Center for Excellence in Nanoscience, Beijing Key Laboratory of Micro-nano Energy and Sensor, Beijing Institute of Nanoenergy and Nanosystems, Chinese Academy of Sciences, Beijing 101400, China; School of Nanoscience and Technology, University of Chinese Academy of Sciences, Beijing 100049, China*

Yuyu Gao – *CAS Center for Excellence in Nanoscience, Beijing Key Laboratory of Micro-nano Energy and Sensor, Beijing Institute of Nanoenergy and Nanosystems, Chinese Academy of Sciences, Beijing 101400, China*

Xiaohan Zhang – *CAS Center for Excellence in Nanoscience, Beijing Key Laboratory of Micro-nano Energy and Sensor, Beijing Institute of Nanoenergy and Nanosystems, Chinese Academy of Sciences, Beijing 101400, China; School of Nanoscience and Technology, University of Chinese Academy of Sciences, Beijing 100049, China*

Guoxu Liu – *CAS Center for Excellence in Nanoscience, Beijing Key Laboratory of Micro-nano Energy and Sensor, Beijing Institute of Nanoenergy and Nanosystems, Chinese Academy of Sciences, Beijing 101400, China; School of Nanoscience and Technology, University of Chinese Academy of Sciences, Beijing 100049, China*

Han Zhou – *CAS Center for Excellence in Nanoscience, Beijing Key Laboratory of Micro-nano Energy and Sensor, Beijing Institute of Nanoenergy and Nanosystems, Chinese Academy of Sciences, Beijing 101400, China; Center on Nanoenergy Research, School of Physical Science and Technology, Guangxi University, Nanning 530004, China*

Yi Lv – *CAS Center for Excellence in Nanoscience, Beijing Key Laboratory of Micro-nano Energy and Sensor, Beijing Institute of Nanoenergy and Nanosystems, Chinese Academy of Sciences, Beijing 101400, China; School of Nanoscience and Technology, University of Chinese Academy of Sciences, Beijing 100049, China*

Complete contact information is available at:
https://pubs.acs.org/10.1021/acsenergylett.1c00704

Author Contributions

[#]X.F. and S.X. contributed equally to this work.

Notes

The authors declare no competing financial interest.

■ ACKNOWLEDGMENTS

The authors thank the support of the National Natural Science Foundation of China (51922023, 61874011), the National Key Research and Development Program of China (2016YFA0202704), the Tribology Science Fund of State Key Laboratory of Tribology (SKLTKF19B02), and the Open Research Foundation of State Key Laboratory of Digital Manufacturing Equipment & Technology (DMETKF2020014).

■ REFERENCES

(1) Paulo e Silva, A. G.; Basílio Sobrinho, J. M.; da Rocha Souto, C.; Ries, A.; de Castro, A. C. Design, Modelling and Experimental Analysis of a Piezoelectric Wind Energy Generator for Low-Power Applications. *Sens. Actuators, A* **2021**, *317*, 112462.
(2) Wang, Q.; Zou, H. X.; Zhao, L. C.; Li, M.; Wei, K. X.; Huang, L. P.; Zhang, W. M. A Synergetic Hybrid Mechanism of Piezoelectric and Triboelectric for Galloping Wind Energy Harvesting. *Appl. Phys. Lett.* **2020**, *117* (4), 043902.
(3) Zhang, L.; Meng, B.; Xia, Y.; Deng, Z.; Dai, H.; Hagedorn, P.; Peng, Z.; Wang, L. Galloping Triboelectric Nanogenerator for Energy Harvesting under Low Wind Speed. *Nano Energy* **2020**, *70*, 104477.
(4) Tian, J.; Chen, X.; Wang, Z. L. Environmental Energy Harvesting Based on Triboelectric Nanogenerators. *Nanotechnology* **2020**, *31*, 242001.
(5) Pan, H.; Li, H.; Zhang, T.; Laghari, A. A.; Zhang, Z.; Yuan, Y.; Qian, B. A Portable Renewable Wind Energy Harvesting System Integrated S-Rotor and H-Rotor for Self-Powered Applications in High-Speed Railway Tunnels. *Energy Convers. Manage.* **2019**, *196* (May), 56–68.
(6) Guo, Y.; Chen, Y.; Ma, J.; Zhu, H.; Cao, X.; Wang, N.; Wang, Z. L. Harvesting Wind Energy: A Hybridized Design of Pinwheel by Coupling Triboelectrification and Electromagnetic Induction Effects. *Nano Energy* **2019**, *60* (April), 641–648.
(7) Fu, X.; Bu, T.; Li, C.; Liu, G.; Zhang, C. Overview of Micro/nano-Wind Energy Harvesters and Sensors. *Nanoscale* **2020**, *12*, 23929–23944.
(8) Dudem, B.; Kim, D. H.; Yu, J. S. Triboelectric Nanogenerators with Gold-Thin-Film-Coated Conductive Textile as Floating Electrode for Scavenging Wind Energy. *Nano Res.* **2018**, *11* (1), 101–113.
(9) Chen, B.; Yang, Y.; Wang, Z. L. Scavenging Wind Energy by Triboelectric Nanogenerators. *Adv. Energy Mater.* **2018**, *8* (10), 1702649.
(10) Fan, X.; He, J.; Mu, J.; Qian, J.; Zhang, N.; Yang, C.; Hou, X.; Geng, W.; Wang, X.; Chou, X. Triboelectric-Electromagnetic Hybrid Nanogenerator Driven by Wind for Self-Powered Wireless Transmission in Internet of Things and Self-Powered Wind Speed Sensor. *Nano Energy* **2020**, *68*, 104319.
(11) Hu, J.; Pu, X.; Yang, H.; Zeng, Q.; Tang, Q.; Zhang, D.; Hu, C.; Xi, Y. A Flutter-Effect-Based Triboelectric Nanogenerator for Breeze Energy Collection from Arbitrary Directions and Self-Powered Wind Speed Sensor. *Nano Res.* **2019**, *12* (12), 3018.
(12) Ren, X.; Fan, H.; Wang, C.; Ma, J.; Li, H.; Zhang, M.; Lei, S.; Wang, W. Wind Energy Harvester Based on Coaxial Rotatory Freestanding Triboelectric Nanogenerators for Self-Powered Water Splitting. *Nano Energy* **2018**, *50* (March), 562–570.
(13) Xi, F.; Pang, Y.; Li, W.; Jiang, T.; Zhang, L.; Guo, T.; Liu, G.; Zhang, C.; Wang, Z. L. Universal Power Management Strategy for Triboelectric Nanogenerator. *Nano Energy* **2017**, *37*, 168–176.
(14) Bae, J.; Lee, J.; Kim, S.; Ha, J.; Lee, B. S.; Park, Y.; Choong, C.; Kim, J. B.; Wang, Z. L.; Kim, H. Y.; Park, J. J.; Chung, U. I. Flutter-Driven Triboelectrification for Harvesting Wind Energy. *Nat. Commun.* **2014**, *5*, 4929.
(15) Fan, F.-R.; Tian, Z.-Q.; Lin Wang, Z. Flexible Triboelectric Generator. *Nano Energy* **2012**, *1* (2), 328–334.
(16) Lin, L.; Xie, Y.; Niu, S.; Wang, S.; Yang, P. K.; Wang, Z. L. Robust Triboelectric Nanogenerator Based on Rolling Electrification

and Electrostatic Induction at an Instantaneous Energy Conversion Efficiency of ~ 55%. *ACS Nano* **2015**, *9* (1), 922−930.

(17) Liu, D.; Yin, X.; Guo, H.; Zhou, L.; Li, X.; Zhang, C.; Wang, J.; Wang, Z. L. A Constant Current Triboelectric Nanogenerator Arising from Electrostatic Breakdown. *Sci. Adv.* **2019**, *5* (4), No. eaav6437.

(18) Pu, X.; Liu, M.; Chen, X.; Sun, J.; Du, C.; Zhang, Y.; Zhai, J.; Hu, W.; Wang, Z. L. Ultrastretchable, Transparent Triboelectric Nanogenerator as Electronic Skin for Biomechanical Energy Harvesting and Tactile Sensing. *Sci. Adv.* **2017**, *3* (5), No. e1700015.

(19) Zhai, N.; Wen, Z.; Chen, X.; Wei, A.; Sha, M.; Fu, J.; Liu, Y.; Zhong, J.; Sun, X. Blue Energy Collection toward All-Hours Self-Powered Chemical Energy Conversion. *Adv. Energy Mater.* **2020**, *10* (33), 2001041.

(20) Jiang, H.; Lei, H.; Wen, Z.; Shi, J.; Bao, D.; Chen, C.; Jiang, J.; Guan, Q.; Sun, X.; Lee, S. T. Charge-Trapping-Blocking Layer for Enhanced Triboelectric Nanogenerators. *Nano Energy* **2020**, *75*, 105011.

(21) Shi, Y.; Wang, F.; Tian, J.; Li, S.; Fu, E.; Nie, J.; Lei, R.; Ding, Y.; Chen, X.; Wang, Z. L. Self-Powered Electro-Tactile System for Virtual Tactile Experiences. *Sci. Adv.* **2021**, *7* (6), No. eabe2943.

(22) Song, Y.; Min, J.; Yu, Y.; Wang, H.; Yang, Y.; Zhang, H.; Gao, W. Wireless Battery-Free Wearable Sweat Sensor Powered by Human Motion. *Sci. Adv.* **2020**, *6* (40), No. eaay9842.

(23) Chen, C.; Wen, Z.; Shi, J.; Jian, X.; Li, P.; Yeow, J. T. W.; Sun, X. Micro Triboelectric Ultrasonic Device for Acoustic Energy Transfer and Signal Communication. *Nat. Commun.* **2020**, *11* (1), 4143.

(24) Zhao, J.; Zhen, G.; Liu, G.; Bu, T.; Liu, W.; Fu, X.; Zhang, P.; Zhang, C.; Wang, Z. L. Remarkable Merits of Triboelectric Nanogenerator than Electromagnetic Generator for Harvesting Small-Amplitude Mechanical Energy. *Nano Energy* **2019**, *61*, 111−118.

(25) Zi, Y.; Guo, H.; Wen, Z.; Yeh, M. H.; Hu, C.; Wang, Z. L. Harvesting Low-Frequency (<5 Hz) Irregular Mechanical Energy: A Possible Killer Application of Triboelectric Nanogenerator. *ACS Nano* **2016**, *10* (4), 4797−4805.

(26) Xu, S.; Fu, X.; Liu, G.; Tong, T.; Bu, T.; Wang, Z.; Zhang, C. Comparison of Applied Torque and Energy Conversion Efficiency between Rotational Triboelectric Nanogenerator and Electromagnetic Generator. *IScience* **2021**, *24* (4), 102318.

(27) Bi, M.; Wu, Z.; Wang, S.; Cao, Z.; Cheng, Y.; Ma, X.; Ye, X. Optimization of Structural Parameters for Rotary Freestanding-Electret Generators and Wind Energy Harvesting. *Nano Energy* **2020**, *75*, 104968.

(28) Zhang, Y.; Zeng, Q.; Wu, Y.; Wu, J.; Yuan, S.; Tan, D.; Hu, C.; Wang, X. An Ultra-Durable Windmill-Like Hybrid Nanogenerator for Steady and Efficient Harvesting of Low-Speed Wind Energy. *Nano-Micro Lett.* **2020**, *12* (1), 175.

(29) Ren, Z.; Wang, Z.; Liu, Z.; Wang, L.; Guo, H.; Li, L.; Li, S.; Chen, X.; Tang, W.; Wang, Z. L. Energy Harvesting from Breeze Wind (0.7−6 M s−1) Using Ultra-Stretchable Triboelectric Nanogenerator. *Adv. Energy Mater.* **2020**, *10* (36), 2001770.

(30) Zeng, Q.; Wu, Y.; Tang, Q.; Liu, W.; Wu, J.; Zhang, Y.; Yin, G.; Yang, H.; Yuan, S.; Tan, D.; Hu, C.; Wang, X. A High-Efficient Breeze Energy Harvester Utilizing a Full-Packaged Triboelectric Nanogenerator Based on Flow-Induced Vibration. *Nano Energy* **2020**, *70*, 104524.

(31) Zhao, X.; Zhang, D.; Xu, S.; Qian, W.; Han, W.; Wang, Z. L.; Yang, Y. Stretching-Enhanced Triboelectric Nanogenerator for Efficient Wind Energy Scavenging and Ultrasensitive Strain Sensing. *Nano Energy* **2020**, *75*, 104920.

(32) Xu, L.; Xu, L.; Luo, J.; Yan, Y.; Jia, B. E.; Yang, X.; Gao, Y.; Wang, Z. L. Hybrid All-in-One Power Source Based on High-Performance Spherical Triboelectric Nanogenerators for Harvesting Environmental Energy. *Adv. Energy Mater.* **2020**, *10* (36), 2001669.

(33) Lu, S.; Gao, L.; Chen, X.; Tong, D.; Lei, W.; Yuan, P.; Mu, X.; Yu, H. Simultaneous Energy Harvesting and Signal Sensing from a Single Triboelectric Nanogenerator for Intelligent Self-Powered Wireless Sensing Systems. *Nano Energy* **2020**, *75*, 104813.

(34) Zhao, T.; Cao, S.; Yang, S.; Guo, R.; Sang, S.; Zhang, H. A Self-Powered Counter/timer Based on a Clock Pointer-like Frequency-Tunable Triboelectric Nanogenerator for Wind Speed Detecting. *Nano Energy* **2019**, *65*, 104025.

(35) Wang, Y.; Wang, J.; Xiao, X.; Wang, S.; Kien, P. T.; Dong, J.; Mi, J.; Pan, X.; Wang, H.; Xu, M. Multi-Functional Wind Barrier Based on Triboelectric Nanogenerator for Power Generation, Self-Powered Wind Speed Sensing and Highly Efficient Windshield. *Nano Energy* **2020**, *73*, 104736.

(36) Han, Q.; Ding, Z.; Sun, W.; Xu, X.; Chu, F. Hybrid Triboelectric-Electromagnetic Generator for Self-Powered Wind Speed and Direction Detection. *Sustain. Energy Technol. Assessments* **2020**, *39*, 100717.

(37) Win Zaw, N. Y.; Roh, H.; Kim, I.; Goh, T. S.; Kim, D. Omnidirectional Triboelectric Nanogenerator Operated by Weak Wind towards a Self-Powered Anemoscope. *Micromachines* **2020**, *11* (4), 414.

(38) Xi, F.; Pang, Y.; Liu, G.; Wang, S.; Li, W.; Zhang, C.; Wang, Z. L. Self-Powered Intelligent Buoy System by Water Wave Energy for Sustainable and Autonomous Wireless Sensing and Data Transmission. *Nano Energy* **2019**, *61*, 1−9.

(39) Zhang, C.; Tang, W.; Han, C. B.; Fan, F. R.; Wang, Z. L. Theoretical Comparison, Equivalent Transformation, and Conjunction Operations of Electromagnetic Induction Generator and Triboelectric Nanogenerator for Harvesting Mechanical Energy. *Adv. Mater.* **2014**, *26* (22), 3580−3591.

https://doi.org/10.1021/acsenergylett.1c00704
ACS Energy Lett. 2021, 6, 2343−2350